Role of volume change on the physics of thermoelectric half-Heusler compounds

M. Yazdani-Kachoei,[1,2,*] S. Li,[3,4] W. Sun,[3,4] S. Mehdi Vaez Allaei,[5,6] and I. Di Marco[1,7,8,†]
[1]Asia Pacific Center for Theoretical Physics, Pohang 37673, Korea
[2]Department of Physics, Faculty of Physics, University of Isfahan, Hezar Jerib Avenue, Isfahan 81746-73441, Iran
[3]SEU-FEI Nano-Pico Center, Key Laboratory of MEMS of Ministry of Education, Southeast University, Nanjing, 210096, Jiangsu, China
[4]Jiangsu Province Key Laboratory of Advanced Metallic Materials, Southeast University, Nanjing, 210096, Jiangsu, China
[5]Department of Physics, University of Tehran, Tehran 14395-547, Iran
[6]School of Nano Science, Institute for Research in Fundamental Sciences, Tehran 19395-5531, Iran
[7]Department of Physics and Astronomy, Uppsala University, Box 516, SE-75120 Uppsala, Sweden
[8]Department of Physics, POSTECH, Pohang 37673, Korea

(Received 22 March 2023; accepted 2 October 2023; published 25 October 2023)

Doping at particular sites is a common method for increasing the thermoelectric efficiency of materials, by tuning carrier concentration and electronic structure. A secondary effect of doping, as well as defects, is to induce a volume change, usually referred to as chemical pressure, that may affect the thermoelectric efficiency. Theoretical investigations usually ignore the role of volume change in thermoelectric improvement, mostly for computational limitations. In this work, we address the role of chemical pressure on the thermoelectric properties of TaFeSb, MOsSb (M = Ta, Nb), and NRuAs (N = Ta, Nb, V) by using *ab initio* electronic structure calculations. We calculate the effect of both negative and positive pressure on the electronic structure, the Seebeck coefficient, electrical and thermal conductivity, as well as the power factor and thermoelectric performance. We argue that volume change, occurring because of defects or doping, should be regarded as an essential parameter to determine the thermoelectric efficiency accurately, as exemplified by TaFeSb. Among the investigated compounds, TaRuAs stands out for the peculiar behavior of electronic and thermoelectric properties with respect to volume change. NbOsSb also stands out, as the sole compounds whose thermoelectric efficiency is maximal in the ground state and cannot be increased via a moderate volume change. Overall, we predict that TaRuAs can be an excellent candidate for thermoelectric applications, due to its large thermoelectric efficiency at zero pressure and the possibility of increasing it by a small volume change. Direct calculations of $TaRuAs_{0.875}Bi_{0.125}$ demonstrate the improved thermoelectric properties while also providing an estimate of the accuracy of our chemical-pressure-based modeling of the doping process.

DOI: 10.1103/PhysRevMaterials.7.104602

I. INTRODUCTION

Thermoelectric materials capable of converting thermal energy into electrical energy, and vice versa, can be exploited as a renewable energy source [1–5]. However, applications of any technology based on these materials have been limited so far, due to their limited efficiency. Thus, tremendous research efforts have been invested to discover new materials with a high thermoelectric efficiency or to improve the currently available materials [3–10]. The thermoelectric efficiency of a material is measured with a dimensionless parameter called the figure of merit, corresponding to $ZT = \sigma S^2 T/\kappa$, where S, σ, T, and κ are, respectively, the Seebeck coefficient, electrical conductivity, temperature, and thermal conductivity [1]. The ZT value of a good thermoelectric material is equal to or greater than unity [11].

Decreasing the thermal conductivity and increasing the power factor ($\mathrm{PF} = \sigma S^2$) are two well-known and broad strategies for improving the ZT parameter. The first goal can be achieved through isoelectronic alloying, nanostructuring, and defects, while the second one may require band-gap engineering and adjusting the carrier concentration. Defects and doping are the main way to vary the carrier concentration, but they also induce a volume compression (expansion), which is often referred to as a positive (negative) chemical pressure [12–16]. Both these effects may in turn affect the thermoelectric efficiency; for instance, previous calculations demonstrated that the enhancement of the Seebeck coefficient observed in Sb_2Te_3 after Bi doping originates from the volumetric changes [17]. Analogously, according to recent theoretical calculations, the ZT value of TiNiSn and LaPtBi can be significantly increased by a volume contraction [18,19]. Govindaraj *et al.* [20] theoretically predicted that, at 750 K, the ZT of $ZnGa_2Te_4$ should increase from about 0.1

*majidyazdani.kachoei@apctp.org
†igor.dimarco@physics.uu.se

Published by the American Physical Society under the terms of the Creative Commons Attribution 4.0 International license. Further distribution of this work must maintain attribution to the author(s) and the published article's title, journal citation, and DOI. Funded by Bibsam.

to 0.77 after applying a hydrostatic pressure of 12 GPa. It is important to highlight that the volume change and the chemical pressure associated with doping may be quite substantial. For example, doping ZnS with 10% Cd results in a volume increase corresponding to a negative chemical pressure of about 2 GPa [21]. In general, values as high as several GPa are achievable by employing elements of different size and higher concentrations [22]. During the past decade, several experimental and theoretical studies were devoted to investigate the effects of volume compression (positive pressure) on the electronic and thermoelectric properties of various materials [18–20,23–26]. Conversely, the effects of volume extension are far less studied, probably based on the expectation that they should act opposite to what is observed for the volume decrease; however, as we will demonstrate in this manuscript, this cannot be considered as a general rule. For instance, our calculations will reveal that the figure of merit of NbOsSb is worsened by both volume compression and extension.

In the ongoing quest for materials with high thermoelectric efficiency, Heusler compounds have received considerable attention [6,27–31]. These materials, discovered by Heusler in 1903, are categorized in half-Heusler (HH) and full-Heusler (FH) compounds, which differ for their crystal structure [32]. While FH compounds are composed of four interpenetrating face-centered-cubic (fcc) lattices, one of them is empty for HH compounds [33]. This difference can lead to a variety of interesting properties. Aliev *et al.* [34–36] were the first to report on the unusual optical and transport properties (including thermoelectricity) of the HH compounds TiMnSn, ZrMnSn, and HfMnSn. The semiconducting nature of these materials, as well as their narrow band structure, were confirmed a few years later through first-principles calculations by Öğüt *et al.* [37]. Since then, it has become clear that the fundamental characteristics of their electronic structure makes HH compounds very interesting for applications in thermoelectricity, spintronics, solar cells, diluted magnetic semiconductors, and topological insulators [38–40]. In 2019, Zhu *et al.* [6] predicted the existence of the HH compounds TaFeSb, MOsSb, and NRuAs, with $M = $ Ta, Nb; $N = $ Ta, Nb, V. TaFeSb was also synthesized and shown to have a surprisingly high thermoelectric efficiency, exceeding that of all other well-known p-type HH compounds [6]. To improve on this impressive achievement, theoretical studies [10,14,30] were conducted to understand the effects of carrier concentration on the thermoelectric properties of HH compounds. Tranås *et al.* [41] have focused on the lattice thermal conductivity, while Zeeshan *et al.* [30] have investigated electronic and phonon properties in great detail. Very recently, Akinlami *et al.* [42] have studied the thermoelectric properties of the NRuAs ($N = $ Ta, V) compounds as a function of carrier concentration, as well as their electronic structures.

All previous studies have addressed the effects associated with varying the carrier concentration on the thermoelectric properties of the HH compounds predicted by Zhu *et al.* [6] by ignoring the volumetric changes resulting from the chemical pressure. To remedy to this issue, we intend to investigate how volume compression and expansion affect the electronic, lattice, and thermoelectric properties of TaFeSb, MOsSb, and NRuAs ($M = $ Ta, Nb; $N = $ Ta, Ru, V) by employing a combination of density-functional theory (DFT) [43,44] and Boltzmann transport theory [45]. The considered negative pressures in this study are available in experiments using doping and defects [14,16], while the positive ones can be achieved experimentally by doping and defects [14], as well as by applying a hydrostatic pressure [18]. The variation of the electronic structure upon volume change is found to be qualitatively different in TaFeSb and TaRuAs with respect to the other compounds under study. The thermoelectric efficiency of TaFeSb, TaOsSb, NbRuAs, and VRuAs is found to increase (decrease) as the volume increases (decreases). A similar result is observed for the thermoelectric efficiency of TaRuAs at low and intermediate temperatures, while at high temperatures a more complex behavior emerges. Our calculations also predict that the best value for thermoelectric efficiency of NbOsSb is found at zero pressure, and any volume variation results in worse properties. Overall, TaRuAs is predicted to be a very efficient thermoelectric material, even better than the previously synthesized TaFeSb. Finally, our analysis of the effects of the chemical pressure is verified by additional calculations for $TaRuAs_{0.875}Bi_{0.125}$, which show a very good agreement with undoped TaRuAs under negative pressure, in agreement with our hypothesis.

The present paper is organized as follows. Section II is dedicated to the methodological details, including the main equations and computational settings. In Sec. III, the electronic properties are described. Thermoelectric properties, including the Seebeck coefficient, electrical conductivity, power factor, thermal conductivity, and figure of merit, are presented in Sec. IV. The results for $TaRuAs_{0.875}Bi_{0.125}$ are illustrated and discussed in Sec. V. The final section includes our conclusion to this study and an outlook for future research. Additional details on the calculations, as well as the results of the optimized lattice parameters and elastic properties, are presented in the Supplemental Material (SM) [46], including also Refs. [47–50] therein.

II. METHODOLOGICAL DETAILS

We carried out electronic structure calculations in the framework of density functional theory (DFT) [43,44], using the full-potential augmented plane-wave plus local orbital (FP-APW+lo) [51] approach, as implemented in the WIEN2K code [52]. The spin-orbit coupling has been included from the outset, since the compounds to investigate are composed of some heavy elements. In addition, past DFT-based studies have demonstrated that the inclusion of spin-orbit coupling is necessary to describe the thermoelectric properties accurately, as the band splitting induced by it affects the electronic transport substantially [53,54]. The calculations of the HH compounds were carried out by considering 165 **k**-points in the irreducible wedge of the first Brillouin zone, corresponding to a Monkhorst-Pack [55] grid of $17 \times 17 \times 17$ points. $TaRuAs_{0.875}Bi_{0.125}$ was instead modeled with a $2 \times 2 \times 2$ supercell, including 24 atoms. Its Brillouin zone was sampled with a Monkhorst-Pack [55] grid of $9 \times 9 \times 9$ points, corresponding to 35 **k**-points in the irreducible wedge. The expansion of the wave functions inside the muffin-tin spheres and interstitial region was done by using cutoff parameters as $R_{\mathrm{MT}}K_{\mathrm{max}} = 7.5$ and $l_{\mathrm{max}} = 10$, where R_{MT} is the radius of the smallest atomic sphere in the unit cell. The periodic charge

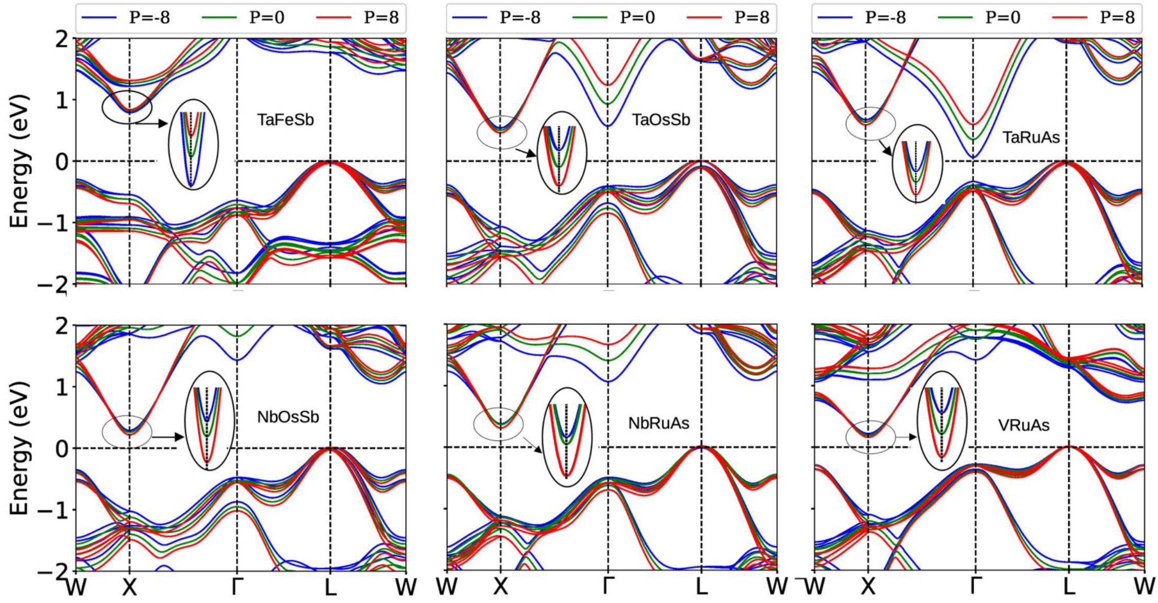

FIG. 1. Band structure of TaFeSb, TaOsSb, TaRuAs, NbOsSb, NbRuAs, and VRuAs at a pressure of −8 GPa (blue lines), 0 GPa (green lines), and 8 GPa (red lines).

density and potential expansions were done with a cutoff parameter $G_{\max}$ equal to 12 a.u.$^{-1}$. Moreover, the exchange-correlation functional was treated in the generalized gradient approximation, as parametrized by Perdew-Burke-Ernzerhof (PBE-GGA) [56].

Effective mass and elastic properties calculations were done using the MSTAR [57] code and IRELAST package [58] of the WIEN2K code, respectively. The results of elastic properties calculations including the elastic constants, Voigt, Reuss, and Hill bulk, shear, and Young's moduli, as well as the transverse, longitudinal, and average wave velocity, and Debye temperature are presented in Tables II–V of the SM [46].

Thermoelectric calculations were performed through the BOLTZTRAP2 code [59], which is based on the semiclassical Boltzmann theory [45]. We performed these calculations in the temperature range from 300 to 1000 K, with steps of 10 K, and using hole carrier concentrations up to 10^{23} cm^{-3}. The BOLTZTRAP2 code [59] uses the following equations to calculate the thermoelectric parameters, including the Seebeck coefficient (S), the electrical conductivity (σ), and the electronic part of thermal conductivity (κ_e):

$$\sigma = \mathscr{L}^{(0)}, \tag{1}$$

$$S = \frac{1}{qT}\frac{\mathscr{L}^{(1)}}{\mathscr{L}^{(0)}}, \tag{2}$$

$$\kappa_e = \frac{1}{q^2T}\left[\frac{(\mathscr{L}^{(1)})^2}{\mathscr{L}^{(0)}} - \mathscr{L}^{(2)}\right], \tag{3}$$

where

$$\mathscr{L}^{(\alpha)}(\mu;T) = q^2\int \sigma(\varepsilon,T)(\varepsilon-\mu)^{\alpha}\left(-\frac{\partial f^0(\varepsilon;\mu,T)}{\partial\varepsilon}\right)d\varepsilon, \tag{4}$$

whereas

$$\sigma(\varepsilon,T) = \int\sum_b \mathbf{V}_{b,\mathbf{k}}\bigotimes\mathbf{V}_{b,\mathbf{k}}\tau_{b,\mathbf{k}}(\varepsilon-\varepsilon_{b,\mathbf{k}})\frac{d\mathbf{k}}{8\pi^3}. \tag{5}$$

In the above equations, $q, \mu, f^0, \tau, \mathbf{V}_{b,\mathbf{k}}$ are the charge of the carriers, chemical potential, Fermi-Dirac distribution function, relaxation time, and group velocity components, respectively. Based on Eqs. (1) and (3)–(5), calculating the σ and κ_e parameters requires the relaxation time τ as input. This parameter can be calculated using the following approximation [19,60]:

$$\tau = \frac{A}{T^{3/2}},\quad A = \frac{2\sqrt{2\pi}C\hbar^4}{3(k_Bm_d^{\star}T)^{3/2}E^2}, \tag{6}$$

where C, $\hbar$, k_B, $m_d^{\star}$, and E are the elastic constant, the reduced Planck constant, the Boltzmann constant, the density-of-states effective mass, and the deformation energy. Calculated C and E parameters are presented in Tables II and VII of the SM [46], respectively. The details and results of the calculations of the relaxation time for the cases under study are instead presented in Sec. IV of the SM [46].

Since $Z = PF/\kappa$, calculating the figure of merit requires both the power factor and the thermal conductivity κ, which includes electronic (κ_e) and lattice (κ_L) contributions. The former can be easily calculated from the electronic transport data, using Eq. (3). The latter would in principle require the full solution of the linearized phonon Boltzmann transport equation (BTE) [61,62]. This approach is very accurate, but also very time-consuming, because of the phonon calculations. An alternative way to estimate κ_L is provided by Slack's equation [63,64]:

$$\kappa_L = \frac{A_L}{T},\quad A_L = A\frac{\bar{M}\delta\Theta^3}{\gamma^2n^{2/3}}, \tag{7}$$

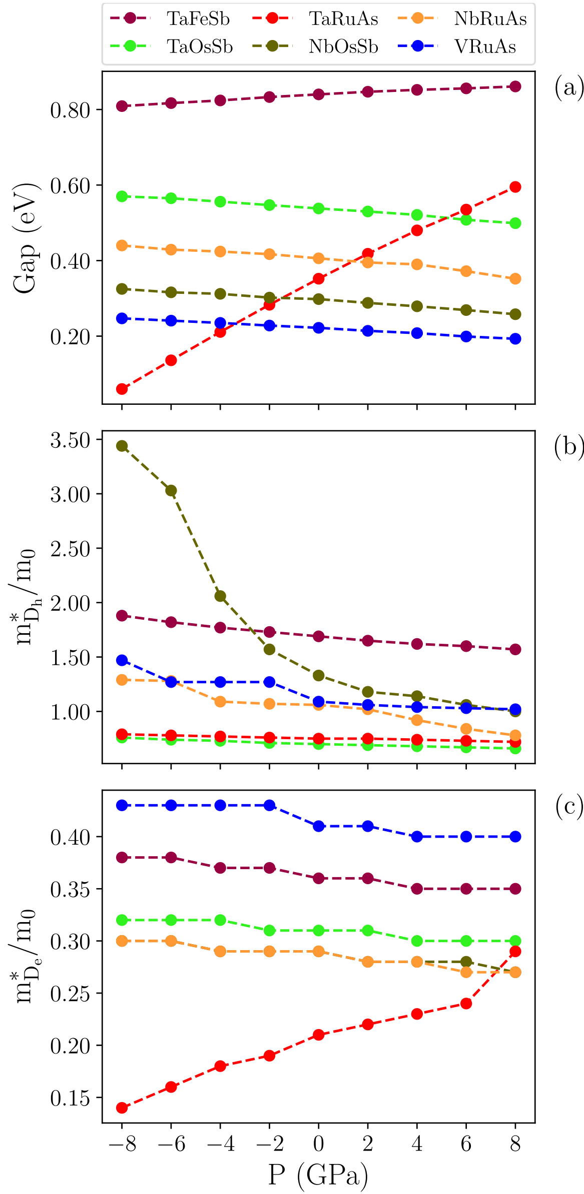

FIG. 2. (a) Band gap of TaFeSb, TaOsSb, TaRuAs, NbOsSb, NbRuAs, and VRuAs upon the variation of pressure; (b) density-of-states effective mass for holes $m^*_{D_h}$ in units of the free-electron mass (m_0); (c) density-of-states effective mass for electrons $m^*_{D_e}$ in units of the free-electron mass (m_0).

where $\bar{M}$, δ, Θ, γ are the average mass of the atoms in the crystal, the volume per atom, the Debye temperature, and the Grüneisen parameter, respectively. A is a constant and amounts to

$$A = \frac{2.43 \times 10^{-8}}{1 - \frac{0.514}{\gamma} + \frac{0.228}{\gamma^2}}.$$

The Grüneisen parameter can be calculated in terms of the Poisson ratio ν:

$$\gamma = \frac{3}{2}\left(\frac{1+\nu}{2-3\nu}\right), \quad \nu = \frac{1-2(v_S/v_L)^2}{2-2(v_S/v_L)^2}, \tag{8}$$

where v_S and v_L are the sound velocities of the longitude and shear waves, respectively. Tiantian Jia and co-workers [63] recently introduced a new, more accurate method to evaluate the Grüneisen parameter, based on the formula

$$\gamma = \sqrt{[\gamma_L^2 + 2\gamma_S^2]/3}. \tag{9}$$

Here, γ_L and γ_S are longitude and shear acoustic Grüneisen parameters [63]:

$$\gamma_L = -\frac{1}{2}\frac{V}{B+4G/3}\frac{\partial(B+4G/3)}{\partial V} - \frac{1}{6}, \tag{10}$$

$$\gamma_S = -\frac{1}{2}\frac{V}{G}\frac{\partial G}{\partial V} - \frac{1}{6}, \tag{11}$$

where B, G, and V are the bulk modulus, shear modulus, and volume of the unit cell, respectively. In this study, we performed most calculations using Slack's equation. To verify the accuracy of our results, we also investigated TaFeSb at zero pressure by using the BTE approach. These calculations were performed by means of the Vienna Ab initio Simulation Package (VASP) [65,66] and the PHONO3PY code [67,68].

Calculations were performed in the pressure range between −8 and 8 GPa, in steps of 2 GPa. These pressures were estimated by fitting the energy versus volume curves with the Murnaghan isothermal equation of state [69]. The optimized volumes, as well as the percent change with respect to the values at zero pressure, are reported in Table I of the SM [46]. For simplicity and computational feasibility, we ignore here the formation of vacancies and antisite defects, which may slightly modify electronic, lattice, and thermoelectric properties of HH compounds [70,71]. In particular, an interesting question arises in relation to the (chemical) pressure dependence of the defect concentration, which may in turn result in a change of the thermoelectric properties of real materials. In this study, we employ the reasonable assumption that these effects are small with respect to those driven by the chemical pressure directly, but we intend to investigate this issue in more detail in future works to provide a more quantitative estimate.

III. ELECTRONIC STRUCTURE

Equations (1)–(5) indicate the relation between thermoelectric properties and electronic structure. As a result, the investigation of the electronic structure is propaedeutic to the analysis of the thermoelectricity. Thus, we calculate the electronic structure of the TaFeSb, MOsSb (M = Ta, Nb), and NRuAs (N = Ta, Nb, V) compounds in PBE-GGA for pressures varying from −8 to +8 GPa.

A. Band structure

The band structures of the compounds under study are displayed in Fig. 1. Let us first focus on the results at zero pressure, i.e., the bands in green. In accordance with previous results [6,10], TaFeSb is a semiconductor with an indirect band gap at zero pressure; the valence-band maximum (VBM) is located at the L point, while the conduction-band minimum (CBM) lies at the X point. A similar result is seen for MOsSb (M = Ta, Nb) and NRuAs (N = Nb, V), with the VBM and CBM located at the L and X points, respectively. TaRuAs is

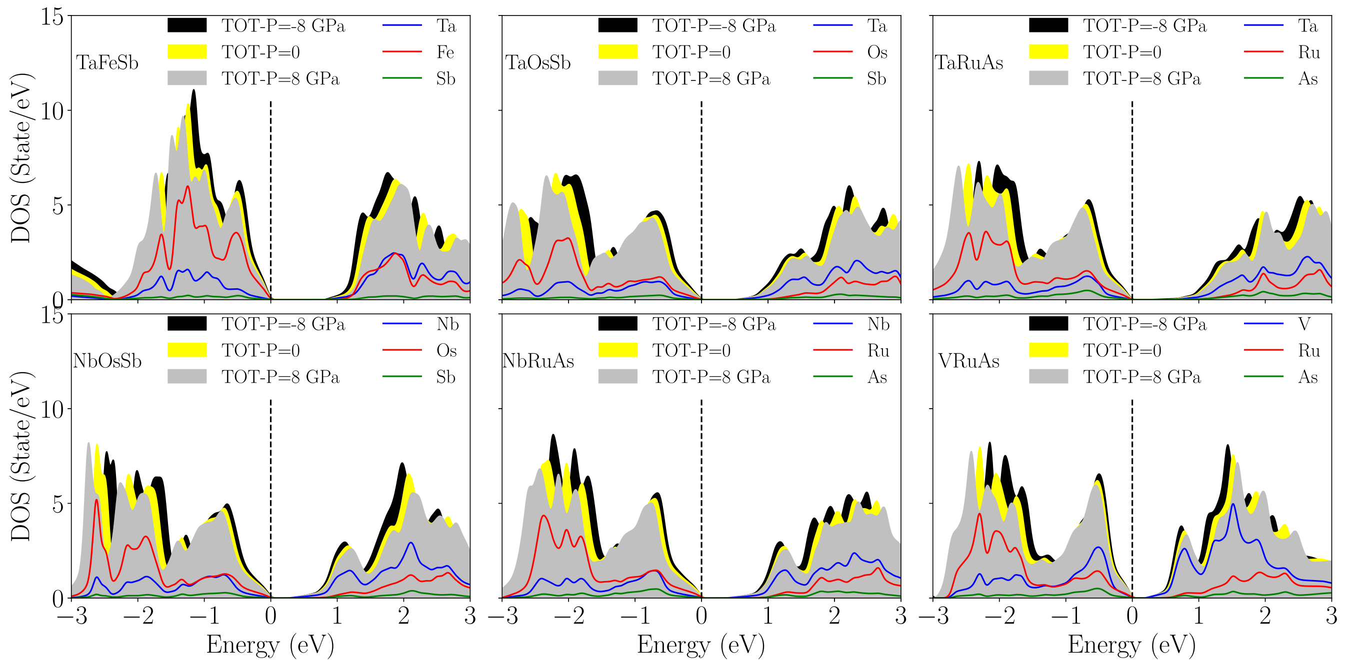

FIG. 3. Total density of states of TaFeSb, TaOsSb, TaRuAs, NbOsSb, NbRuAs, and VRuAs at a pressure of −8, 0, and 8 GPa, along with the atomically projected contributions at zero pressure. The Fermi level is at zero energy.

also found to be a semiconductor with an indirect band gap at zero pressure. Like the other compounds, the VBM is located at the L point, but the CBM lies instead at the Γ point.

The band-gap values versus pressure are plotted in Fig. 2. Our calculations reveal that, at zero pressure, TaFeSb exhibits the highest value, while the lowest one belongs to VRuAs. The experimental value of the band gap of TaFeSb at zero pressure [6], which is the sole value accessible from experimental data, is reported in Table VI of the SM [46]. We can see that this value is about two-thirds of our theoretical value of 0.84 eV for TaFeSb at zero pressure, which is a rather large discrepancy. Conversely, our computed value is in excellent agreement with previous calculations [6,10,14,30,72]. Although one is tempted to attribute the discrepancy between theory and experiment to an approximated exchange-correlation functional, previous calculations based on the modified Becke-Johnson (mBJ) exchange potential [73,74] produced an even worse agreement [6]. This issue is reported in other families of HH compounds as well, and it has been convincingly attributed to disorder and defects. For example, the presence of interstitial Ni (Co) defects in NbCoSn, TiCoSb, ZrNiSn, and TiNiSn has been demonstrated to explain the discrepancy between theoretical and experimental band gap, as well as the n-type behavior of these materials [75]. Similarly, antisite defects were shown to play an important role in ZrNiSn [70].

In addition to the band gap, Fig. 2 displays the density-of-states effective mass for holes ($m^{\star}_{D_h}$) and electrons ($m^{\star}_{D_e}$). Our calculated $m^{\star}_{D_h}$ and $m^{\star}_{D_e}$ for TaFeSb at zero pressure are in good agreement with previous theoretical data [10]. Our results show that TaFeSb and VRuAs have the highest value of $m^{\star}_{D_h}$ and $m^{\star}_{D_e}$ at zero pressure, while their lowest values are found for TaOsSb and TaRuAs. Overall, the values of the density-of-states effective mass across the materials are pretty diverse and difficult to predict without a direct calculation of the electronic structure.

Now we turn to the effects of volume change on the electronic structures. Comparing the band structures at different pressures in Fig. 1 reveals that the VBM location in the Brillouin zone does not depend on the volume (in the calculated range of pressure). Similar results have been reported for other HH compounds as well [10,31]. The CBM exhibits the same invariant behavior for TaFeSb, MOsSb (M = Ta, Nb), and NRuAs (N = Nb, V), being located at the X point for all the calculated pressures; however, the CBM of TaRuAs is located at the Γ point for pressures between −8 and 6 GPa, but it moves to the X point when the pressure becomes equal to or higher than 6 GPa. These changes are reflected by the evolution of band-gap values upon varying pressure, reported in Fig. 2. The band gap is found to be a descending function of pressure for MOsSb (M = Ta, Nb) and NRuAs (N = Nb, V). Previous calculations [76] have reported a similar pressure dependence of the band gap for another HH compound, namely LiScSi. In contrast to these compounds, the band gap of TaFeSb increases from 0.81 to 0.86 eV when pressure is increased from −8 to 8 GPa. A similar albeit more marked trend is observed for TaRuAs. This trend of a rising band gap versus pressure has been previously reported for other HH compounds as well, namely ZrXBi (X = Co, Rh) [14], LuPtSb [77], and LaPtBi [19]. Interestingly, the band gap of TaRuAs seems considerably more sensitive to a pressure variation than all other compounds. This behavior is so marked that the band gap of TaRuAs increases from 0.06 eV (the lowest band gap among all our calculations) at −8 GPa to 0.6 eV (the second highest band gap among all our calculations) at 8 GPa.

We now proceed to the analysis of the density-of-states effective mass upon pressure. As visible in Fig. 2, $m^{\star}_{D_h}$ decreases as volume decreases for all compounds under study.

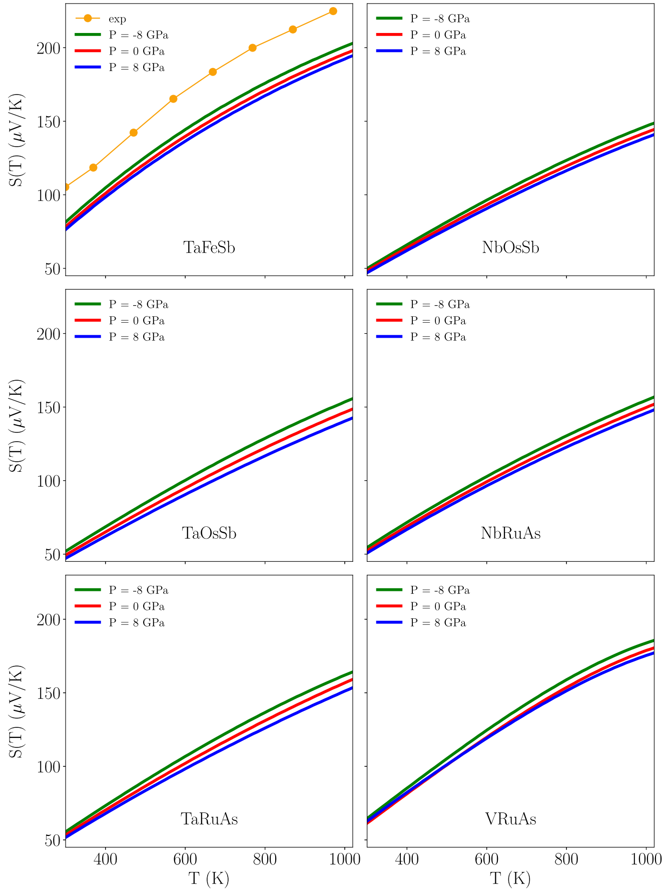

FIG. 4. Seebeck coefficient S of TaFeSb, TaOsSb, TaRuAs, NbOsSb, NbRuAs, and VRuAs vs temperature, for pressures of −8, 0, and 8 GPa and a carrier concentration $n = 20 \times 10^{20}$ cm^{-3}. Experimental results [6] for $Ta_{0.84}Ti_{0.16}FeSb$ at zero pressure are also shown.

For NbOsSb, $m^{\star}_{D_h}$ is much more sensitive to the volumetric changes than for the other compounds. NbOsSb is also found to have the largest value of $m^{\star}_{D_h}$ among all calculations, for a pressure of −8 GPa. Proceeding to the electronic excitations, $m^{\star}_{D_e}$ is found to decrease when pressure is increased for all materials except TaRuAs. Our results reveal that VRuAs has the highest value of $m^{\star}_{D_e}$ at all pressures, while TaRuAs exhibits the lowest value up to 6 GPa and is overcome by Nb-based compounds at 8 GPa. An interesting feature of these plots is that the values of $m^{\star}_{D_e}$ in NbOsSb and NbRuAs remain identical over the whole range of pressures, suggesting a marginal role of the electronic states that do not derive from Nb, as discussed in the next section.

B. Density of states

Figure 3 shows the calculated density of states (DOS) for TaFeSb, MOsSb (M = Ta, Nb), and NRuAs (N = Ta, Nb, V), at pressures of −8, 0, and +8 GPa. The projected DOS's per atom are also displayed for zero pressure only. For TaFeSb, both the valence- and conduction-band regions are dominated by Fe-derived and Ta-derived states. The Sb-derived states do not provide any substantial contribution around the Fermi energy. Hence, doping at the Ta or Fe sites can affect both valence and conduction bands, while doping at the Sb sites can change the carrier concentration without any modification of the electronic structure. Also for MOsSb (M = Ta, Nb), the Sb-derived states do not contribute to the valence and conduction bands effectively. In these compounds, the valence band is dominated by Os- and M-derived states, while only the latter contribute to the conduction band in the vicinity of the Fermi energy. Similar results are observed for NRuAs (N = Ta, Nb, V), where the N-derived states dominate the conduction band at low excitation energies, and As-derived states offer a small contribution to both bands, if compared to the other atomic states. According to these results, the electronic structure of both the valence and conduction bands can be modified by doping MOsSb (M = Ta, Nb) compounds at the M and Os sites and doping NRuAs (N = Ta, Nb, V) compounds at the N and Ru sites, with M. On the contrary, doping at Sb or As can change the carrier concentration without modifying the band structure significantly. Comparing the results at different pressures reveals that volume change has a small effect on the general shape of the DOSs for all investigated materials. As expected, a positive pressure results in wider bands and larger gaps, indicating an increased tendency toward delocalization. The opposite effect is naturally observed for a negative pressure.

IV. THERMOELECTRIC PROPERTIES

We then proceed to the analysis of the thermoelectric properties. The Seebeck coefficient, electrical conductivity, power factor, thermal conductivity, and thermoelectric efficiency are each discussed in the following subsections.

A. Seebeck coefficient

To validate our calculations, let us first compare our results with available experimental data. The thermoelectric performance of TaFeSb was found to achieve a peak ZT of 1.39 at zero pressure and for a 16% doping of Ti at the Ta sites, which corresponds to a carrier concentration of $n = 20 \times 10^{20}$ cm^{-3} [6]. Thus, a good comparison can be made between their Seebeck coefficient and our calculated values for TaFeSb at zero pressure, using the estimated carrier concentration. Theoretical and experimental curves are reported in the top left panel of Fig. 4, showing trends that are in good agreement with each other. Quantitatively, the values are a bit different, with theory underestimating the experimental values by about 25%. This difference can be related to differences in the electronic structure, i.e., to the aforementioned overestimation of the band gap, discussed in Sec. III A. However, it is not the only possible explanation, as we can infer after examining the dependence of the Seebeck coefficient upon volumetric changes. Calculations with positive and negative pressure show that there is a direct relation between $S(T)$ and volume; see the top-left panel of Fig. 4. Increasing the volume, i.e., applying a negative pressure, produces a small increase of the Seebeck coefficient. Thus, the results at a pressure of −8 GPa are closer to the experimental curve than those at zero pressure. This effect is in accordance with the fact that Ti-doping was found to increase the lattice parameters for concentrations larger than 6% in recent experiments [14]. This

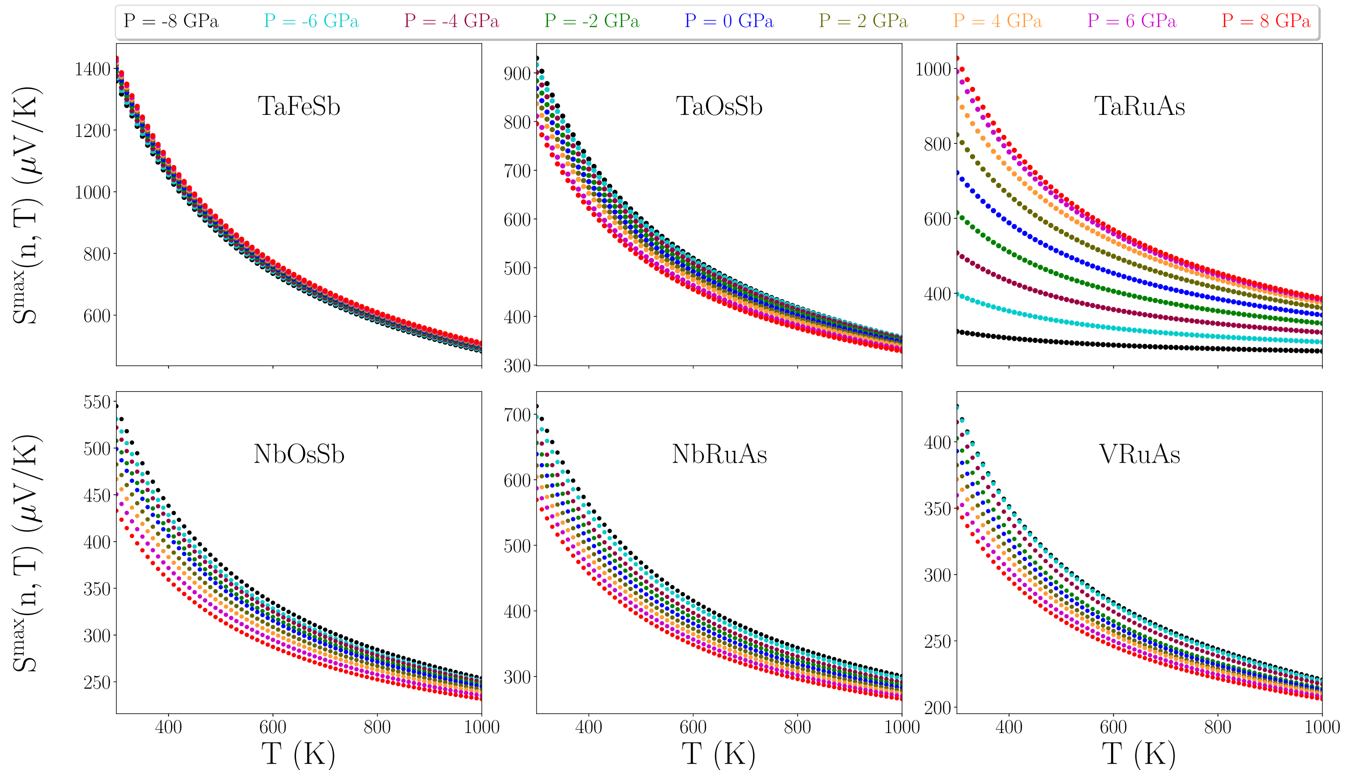

FIG. 5. Maximum value of the Seebeck coefficient ($S^{\max}$) for TaFeSb, TaOsSb, TaRuAs, NbOsSb, NbRuAs, and VRuAs with respect to a varying carrier concentration, as a function of temperature and for pressures from −8 to 8 GPa.

is also in line with what was predicted by Vegard's law for binary alloys of various kinds [12].

For the sake of comparison, we carried out similar calculations for the rest of the compounds, using the same value of carrier concentration. As shown in Fig. 4, the change of the Seebeck coefficient with respect to the temperature or the volume is similar in all compounds. Figure 4 also reveals that the Seebeck coefficient of TaFeSb is noticeably higher than that of the other compounds at all considered pressures for the employed carrier concentration.

Since, according to the ZT formula, increasing the Seebeck coefficient can improve the thermoelectric efficiency, let us investigate the maximum Seebeck coefficient ($S^{\max}$) found upon varying the carrier concentration up to 10^{22} cm^{-3}. This calculation was performed by using the method presented in our previous works [23,24]. $S^{\max}$ versus temperature is reported in Fig. 5 for various values of pressure. The results for 300, 700, and 1000 K are also tabulated in Table IX of the SM [46] for the sake of completeness. By comparing Figs. 5 and 2, we notice that the behavior of $S^{\max}$ versus pressure is very similar to the behavior of the band gap. This observation is in accordance with the Goldsmid-Sharp relation [78]. According to Fig. 5, a rising pressure increases $S^{\max}$ for TaFeSb and TaRuAs, but decreases it for TaOsSb, NbOsSb, and NbRuAs at all considered temperatures. A similar trend is observed for the band gaps shown in Fig. 2. In addition, we note that the $S^{\max}$ of TaFeSb is much higher than that of the other compounds for all considered pressures and temperatures, which reflects the largest band gap discussed in Sec. III A. Similarly, the greater sensitivity of the band gap of TaRuAs to a variation of pressure is reflected by the greater range spanned by the corresponding curves in Fig. 5.

B. Electrical conductivity

The calculated values of σ for $n = 20 \times 10^{20}$ cm^{-3} at −8, 0, and 8 GPa are shown in Fig. 6. In practical terms, the values of σ are calculated by multiplying the output of the BoltzTraP2 code [59] times τ, which is in turn calculated using Eq. (6). For completeness, the calculated values of τ are reported in Table VIII of the SM [46]. Inspecting Eqs. (1) and (2), we expect the Seebeck coefficient and σ to have opposite trends with respect to temperature and pressure. This is precisely what is observed in Fig. 6. Furthermore, the highest and lowest values of σ belong to TaOsSb and TaFeSb, respectively. This result does not depend on the pressure value, as Figure 6 demonstrates.

Figure 6 also includes the available experimental results for $Ta_{0.84}Ti_{0.16}FeSb$ at zero pressure. Comparison with our theoretical data reveals that the consistency between theory and experiment increases with the temperature, both in absolute and relative terms. As for the Seebeck coefficient, the experimental values of σ for $Ta_{0.84}Ti_{0.16}FeSb$ are closer to the theoretical ones for TaFeSb at −8 GPa, which we attribute to volumetric effects associated with doping, at least partially. We should remark, however, that another possible source of discrepancy between theory and experiment for σ may be the

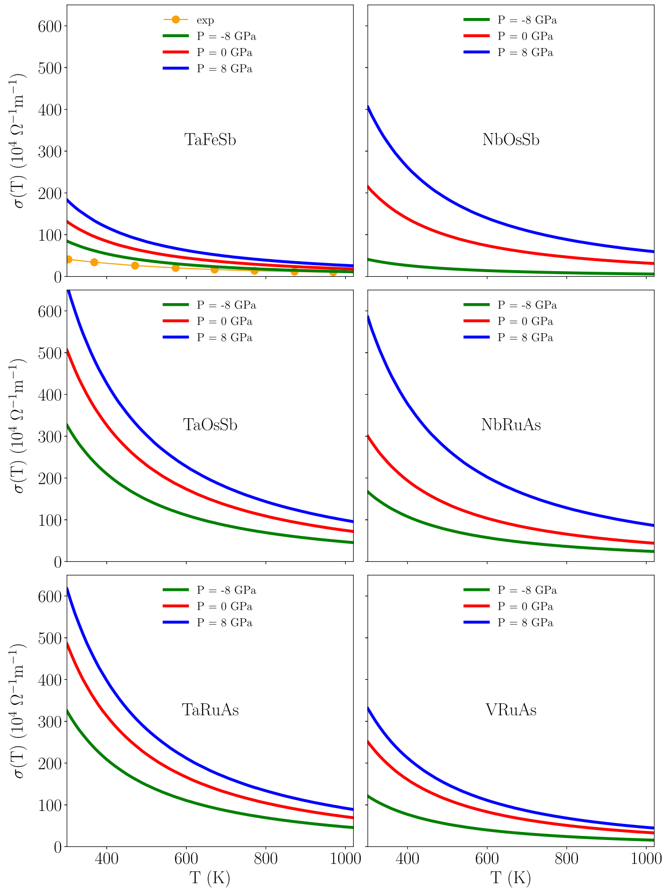

FIG. 6. Electrical conductivity (σ) of TaFeSb, TaOsSb, TaRuAs NbOsSb, NbRuAs, and VRuAs as a function of temperature for various pressures and for a carrier concentration $n = 20 \times 10^{20}$ cm^{-3}. Experimental results [6] for $Ta_{0.84}Ti_{0.16}FeSb$ at zero pressure are also shown.

fact that the relaxation time τ is obtained via Eq. (6), which is an approximation.

Finally, we calculated the temperature dependence of the maximum values of the electrical conductivity (σ^{max}) with respect to varying the carrier concentration. These results are presented in Fig. 7 for pressures between −8 and 8 GPa. For completeness, numerical values at 300, 700, and 1000 K are also reported in Table X of the SM [46]. Independently of the particular compound, σ^{max} is found to increase when pressure is increased, for all temperatures. This reflects a larger bandwidth, which was already discussed in the analysis of Fig. 3. Moreover, TaOsSb and TaRuAs have the highest values of σ^{max} for all considered pressures, while NbOsSb and TaFeSb have the lowest values for pressures up to −4 GPa and larger than −4 GPa, respectively.

C. Power factor

The calculated power factor ($\text{PF} = \sigma S^2$) of TaFeSb, TaOsSb, TaRuAs, NbOsSb, NbRuAs, and VRuAs as a function of temperature for $n = 20 \times 10^{20}$ cm^{-3} is illustrated in Fig. 8. Pressures in the range from −8 to 8 GPa are shown, alongside available experimental data for $Ta_{0.84}Ti_{0.16}FeSb$ at zero pressure [6]. Both theoretical and experimental curves of TaFeSb show a peak at intermediate temperatures. A similar behavior is observed for the other compounds as well. In analogy to S and σ, the experimental PF of $Ta_{0.84}Ti_{0.16}FeSb$ at zero pressure is closer to the theoretical PF of TaFeSb at −8 GPa. As for σ, the PF of all compounds increases when pressure is increased for $n = 20 \times 10^{20}$ cm^{-3}.

The temperature dependence of the maximum values of the power factor (PF^{max}) with respect to the carrier concentration is illustrated in Fig. 9 for various pressures. Tabulated results for 300, 700, and 1000 K are displayed in Table XI of the SM [46]. For all compounds, we observe that PF^{max} increases with pressure, at any temperature within our investigated range. The PF^{max} of NbOsSb seems considerably more sensitive to pressure than the other systems; increasing the pressure from −8 to 8 GPa makes it around 8.5 times larger. Figure 9 also indicates that TaRuAs has the highest PF^{max} in our study, including the whole range of pressures and temperatures. Therefore, from the power factor point of view, TaRuAs is the best thermoelectric material among the compounds we studied. Additionally, our results show that the temperature dependence of PF^{max} depends on the compound. As temperature increases, PF^{max} decreases for TaFeSb, but it increases for TaOsSb, NbOsSb, and NbRuAs. On the other hand, the PF^{max} of TaRuAs is approximately temperature-independent; for example, raising the temperature from 300 to 1000 K results in a small increase of 1.2 μW/cm K^2 at zero pressure.

D. Thermal conductivity

The total thermal conductivity (κ_{tot}) requires both electronic (κ_e) and lattice (κ_L) contributions. For simplicity, the following discussion is focused only on κ_L, since κ_e behaves similarly to σ, due to the Wiedemann-Franz law [1]. The temperature-dependent values of κ_L for all compounds under study and pressures from −8 to 8 GPa are illustrated in Fig. 10. To verify the accuracy of our results based on Slack's equation, we also performed selected calculations for TaFeSb at zero pressure by means of the BTE method, as discussed in Sec. II. An analysis of these results (data not shown) demonstrates that using Slack's equation in these compounds tends to underestimate the theoretical κ_L of less than 20%. This discrepancy is smaller than previously reported by Naydenov *et al.* [10], a disagreement that we can trace back to the method used for the calculation of the Grüneisen parameters. While Naydenov *et al.* [10] employ the Poisson ratio method, we use the more accurate method by Jia *et al.* [63]. Another source of difference is the Debye temperature Θ_D, as reported in Table V of the SM [46]. Proceeding to the analysis of the results, Fig. 10 illustrates that the lowest value of κ_L is found for TaRuAs, independently of pressure and temperature. Therefore, TaRuAs is the best compound for thermoelectric applications among those investigated, in relation to both PF and κ_L. Furthermore, by comparing κ_L at different pressures, we find that the calculated values decrease considerably when volume is increased for all compounds. Finally, Fig. 11 illustrated the total thermal conductivity, including also the electronic contribution for $n = 20 \times 10^{20}$ cm^{-1}, of TaFeSb. For the sake of comparison, the available experimental data [6] for $Ta_{0.84}Ti_{0.16}FeSb$ at zero pressure are also reported. Similarly to what was discussed in

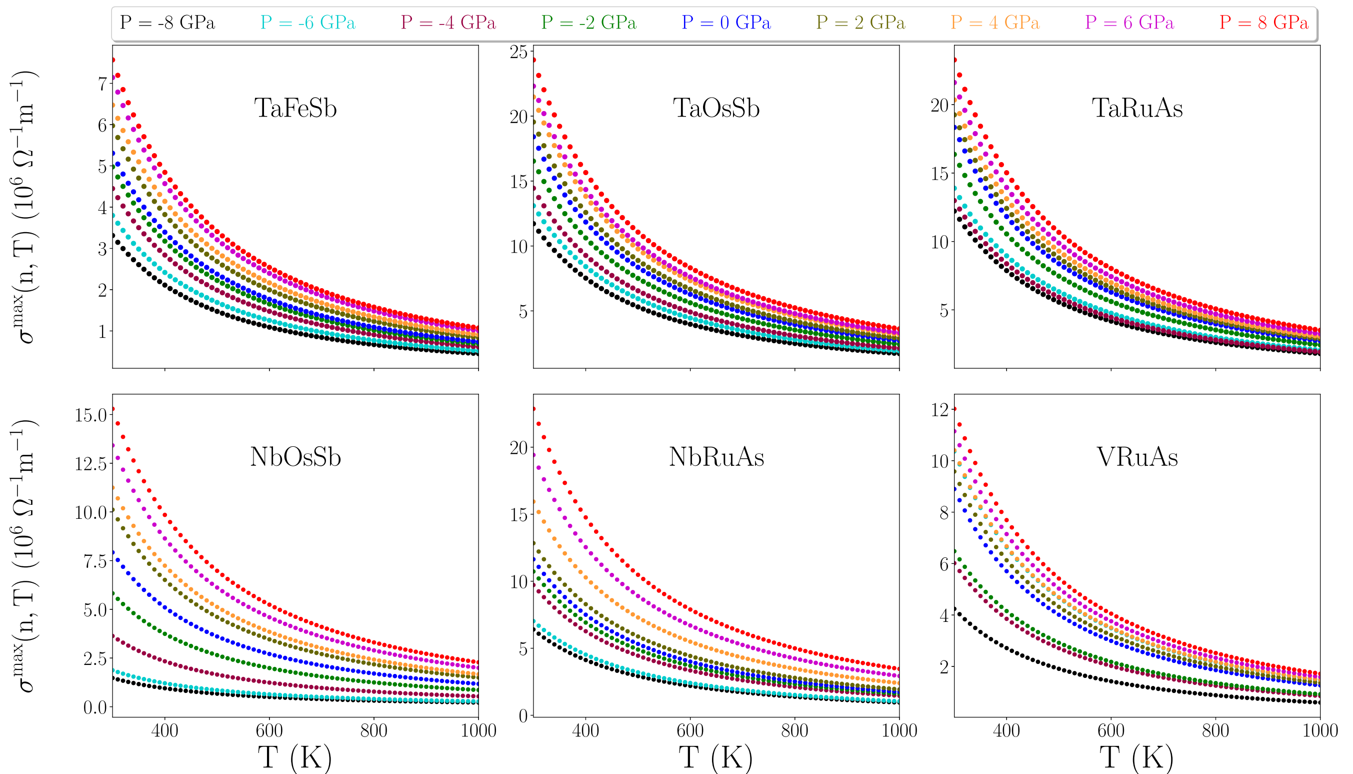

FIG. 7. Maximum value of the electrical conductivity (σ^{max}) for TaFeSb, TaOsSb, TaRuAs, NbOsSb, NbRuAs, and VRuAs with respect to a varying carrier concentration, as a function of temperature and for pressures from −8 to 8 GPa.

the previous sections, this comparison reveals the role played by the volume change induced by doping when comparing theory and experiment.

E. Thermoelectric efficiency

As discussed in the Introduction, the thermoelectric efficiency is measured using the figure of merit ZT. Figure 12 displays the values of ZT versus temperature for the considered materials, for various pressure and for $n = 20 \times 10^{20}$ cm^{-3}. The results for TaFeSb can be compared to the available experimental data for $Ta_{0.84}Ti_{0.16}FeSb$ at zero pressure [6]. The best agreement is again found for the smallest considered volume, for a pressure of −8 GPa, where the discrepancy between theory and experiment amounts to about 20% over the temperatures from 300 to 1000 K. This agreement seems better than those found in the previous sections and arises from error cancellation, due to S and σ being, respectively, underestimated and overestimated. This suggests that the final results on the thermoelectric efficiency of all materials may provide a reliable guideline for experimental investigations and further optimization. Proceeding to cross-compound comparison, Fig. 12 reveals that, for this carrier concentration, the ZT of TaFeSb is more sensitive to volumetric changes than the other systems under study; at 300 K, the ZT of TaFeSb changes by about 0.1 when pressure goes from −8 to 8 GPa, while this change amounts to 0.03–0.05 for the remaining compounds.

We also calculated the optimum values of the figure of merit ($Z^{max}T$) with respect to the carrier concentration. These results are presented in Fig. 13 as a function of temperature and for various pressures. For completeness, the data for 300, 700, and 1000 K are also reported in Table XII of the SM [46]. Our calculations reveal that the $Z^{max}T$ of TaFeSb increases if temperature is increased or upon volume extension. A similar result is seen for TaOsSb, NbRuAs, and VRuAs. A rising temperature results in an increase of $Z^{max}T$ also for TaRuAs and NbOsSb; however, their trend with respect to a change of pressure is different from the other compounds. As can be seen in Fig. 13, volume reduction decreases the $Z^{max}T$ of TaRuAs for low and medium temperatures, while at higher temperatures the curves start crossing each other. We traced back this irregular behavior to the difference in steepness of κ_L for different pressures. As Fig. 1 in the SM [46] reveals, if κ_L is ignored, the ZT of TaRuAs exhibits a regular decrease when the volume is decreased. This irregular behavior was also previously reported for SmTe, another known thermoelectric material [26]. The $Z^{max}T$ of NbOsSb exhibits also a completely different behavior from the others. It increases if pressure is increased from −8 to 0 GPa, but then decreases if pressure is further increased, up to 8 GPa. This means that either volume reduction or volume extension with respect to the ground state worsen the optimum figure of merit.

Making a comparison between $Z^{max}T$ across all compounds reveals that the highest value of this parameter belongs to TaRuAs at low and intermediate temperatures, independently of the pressure value. Conversely, at high temperatures, also the external pressure plays a role. For example, at 1000 K, TaOsSb has the highest value of ZT between −8 and −6 GPa,

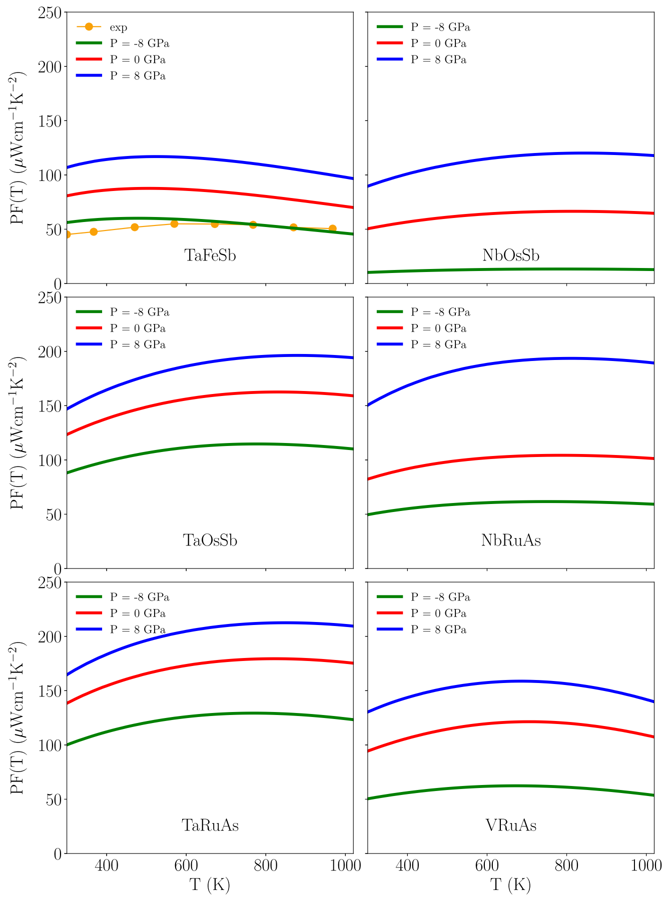

FIG. 8. Calculated power factor (PF) of TaFeSb, TaOsSb, TaRuAs, NbOsSb, NbRuAs, and VRuAs as a function of temperature, for various pressures and for a carrier concentration $n = 20 \times 10^{20}$ cm^{-3}. Experimental results [6] for $Ta_{0.84}Ti_{0.16}FeSb$ at zero pressure are also shown.

while TaRuAs becomes more prominent for pressures larger than −6 GPa.

V. A REALISTIC TEST-CASE

While our discussion suggests that changing pressure and carrier concentration may lead to a significant increase in the maximum figure of merit, it is unclear to what extent the quantum effects associated with chemical doping are going to modify the electronic structure directly. To investigate these effects, we studied a concrete test-case for the most interesting compound identified above, namely TaRuAs. As illustrated in Fig. 13, the $Z^{\max}T$ of TaRuAs is improved by a volume increase at low and intermediate temperature values. A suitable option to obtain a volume increase without affecting the carrier concentration is doping with Bi at the As site. In fact, previous computational studies showed that TaRuBi is likely to be synthesized [79]. In addition, it was shown experimentally [80] that TiCoSb can be doped with Sn at the Sb site, which is analogous to our suggestion for TaRuAs. Based on these results, we expect that $TaRuAs_{1-x}Bi_x$ may be easily accessible in experiments. For computational convenience, we modeled a Bi concentration of 12.5%, which allows for a relatively small supercell, as described in Sec. II. Although this approach makes the problem treatable, the effects of disorder are ignored, which may introduce some errors in determining the thermoelectric properties accurately [81,82]. However, these errors are smaller than the effect of chemical doping we are trying to assess, as they are a direct consequence of it. Thus, this approximation will not affect the purpose of our analysis.

The structural relaxation of the supercell shows that a 12.5% concentration of Bi increases the volume of undoped TaRuAs by about 2.26%, which is very close to the volume obtained for a pressure of −4 GPa. Thus, we first compare the electronic structure of $TaRuAs_{0.875}Bi_{0.125}$ with that of TaRuAs at −4 GPa [46]. The corresponding curves for the DOS are illustrated in Fig. 14. Overall, both the valence and conduction bands of $TaRuAs_{0.875}Bi_{0.125}$ seem slightly wider than those of undoped TaRuAs at −4 GPa. The main peaks are a bit smeared, which is an effect of the quantum interference associated with the different atomic species introduced in the lattice. These small differences are mainly noticeable at intermediate excitation energy, while the region around the Fermi level, which determines the transport properties, is remarkably similar. In accordance with the observed band widening, the band gap of $TaRuAs_{0.875}Bi_{0.125}$ has a value of 0.27 eV, which is closer to the value obtained for undoped TaRuAs at −2 GPa (0.28 eV) than to that at −4 GPa (0.21 eV). These results may be understood by considering that the local structural modifications due to the Bi impurities affect mainly the region around the impurities, while the interatomic distances around the As atoms far from them tend to recover the original values of undoped TaRuAs at zero pressure [12,12]. Therefore, the reduction of the band gap caused by chemical doping may be smaller than that obtained by applying an equivalent chemical pressure on the undoped material. For the sake of completeness, we also plot the DOS for TaRuAs at −2 GPa in Fig. 14.

The thermoelectric properties calculated for $TaRuAs_{0.875}Bi_{0.125}$, including $S^{\max}$, $\sigma^{\max}$, κ_L, and $Z^{\max}T$, are displayed in Fig. 15. For comparison, the corresponding data for undoped TaRuAs at a pressure of 0, −2, and −4 GPa are also shown. As we can see in panels (a) and (b), both $S^{\max}$ and $\sigma^{\max}$ are worsened by Bi doping, in agreement with our prediction based on the chemical pressure alone. Concerning $\sigma^{\max}$, the curve of $TaRuAs_{0.875}Bi_{0.125}$ is almost perfectly coincident with that of undoped TaRuAs at −4 GPa. Conversely, the results for $S^{\max}$ are comprised between the curves for undoped TaRuAs at −2 and −4 GPa. As illustrated in panel (c), alloying with Bi leads to a marked reduction of the lattice thermal conductivity, even larger than what is expected from our predictions. This is due to the changes induced in the phonon spectrum by the Bi impurities, which are detrimental for the propagation of the vibrations along the lattice [83–85]. Quantitatively, the lattice thermal conductivity of $TaRuAs_{0.875}Bi_{0.125}$ is closest to that of undoped TaRuAs at −4 GPa. Finally, in panel (d), we can observe how $Z^{\max}T$ behaves for the different systems considered. We can see that our model based on the concept of chemical pressure alone gives a very good agreement with the direct calculations for $TaRuAs_{0.875}Bi_{0.125}$. The best agreement is obtained for a chemical pressure of −2 GPa, with some small differences appearing only for temperatures between 700 and 1000 K. The data for −4 GPa are also in very good agreement with

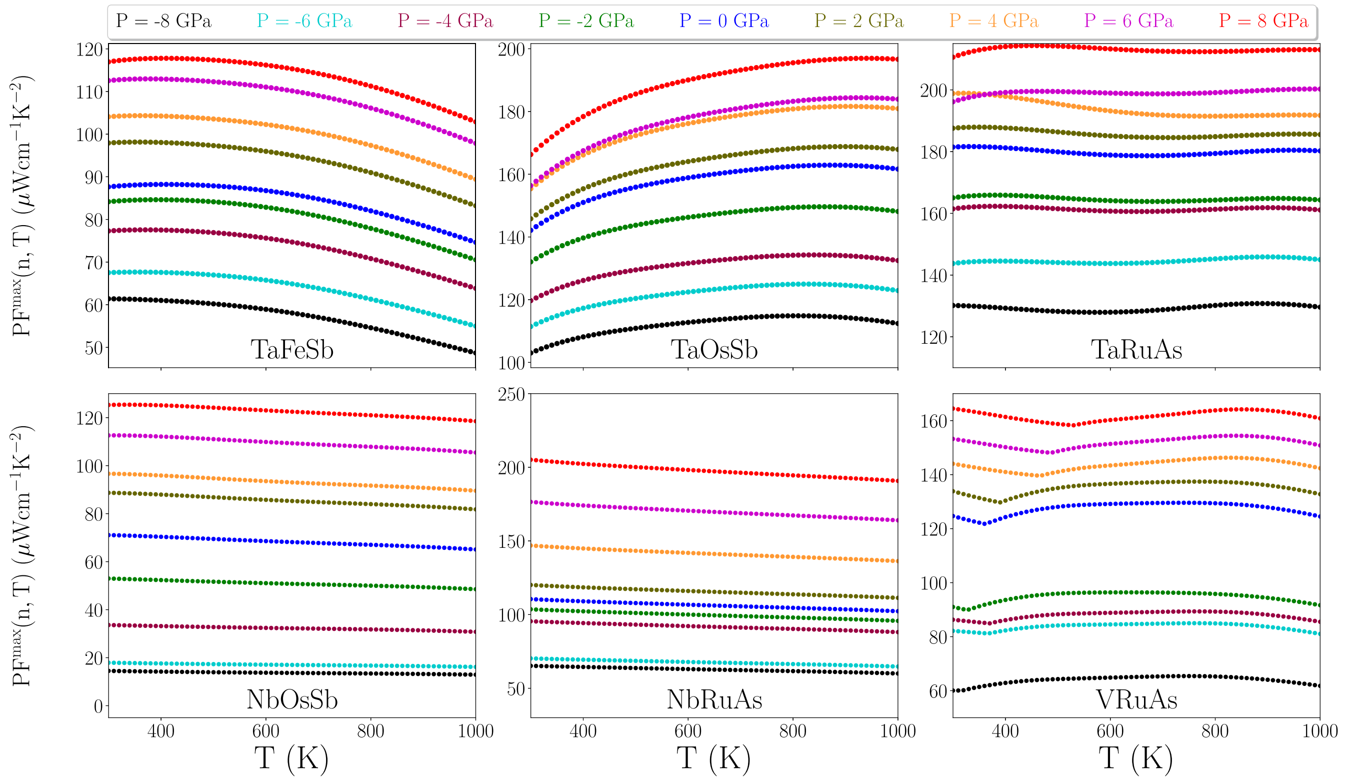

FIG. 9. Maximum value of the power factor (PF^{max}) for TaFeSb, TaOsSb, TaRuAs, NbOsSb, NbRuAs, and VRuAs with respect to a varying carrier concentration, as a function of temperature and for pressures from −8 to 8 GPa.

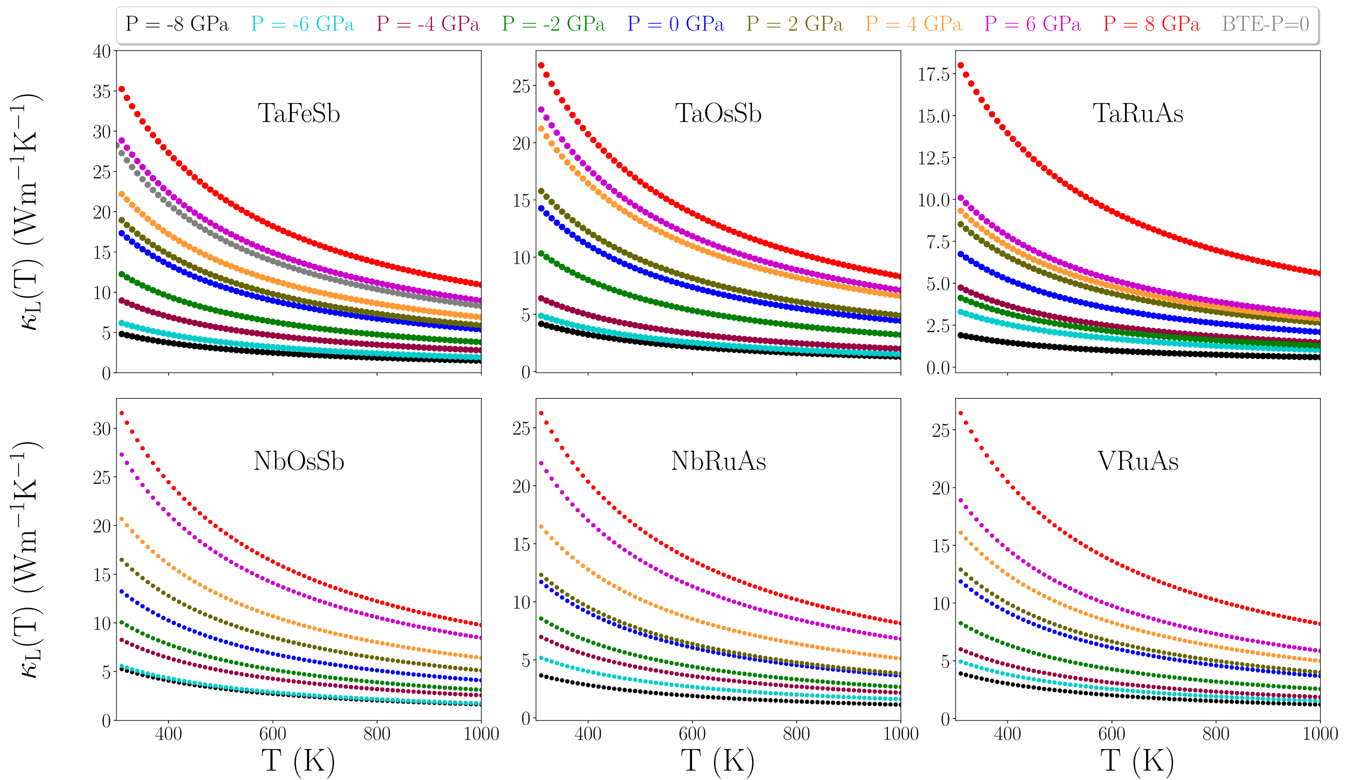

FIG. 10. Calculated lattice thermal conductivity (κ_L) of TaFeSb, TaOsSb, TaRuAs NbOsSb, NbRuAs, and VRuAs as a function of temperature, for pressures from −8 to 8 GPa.

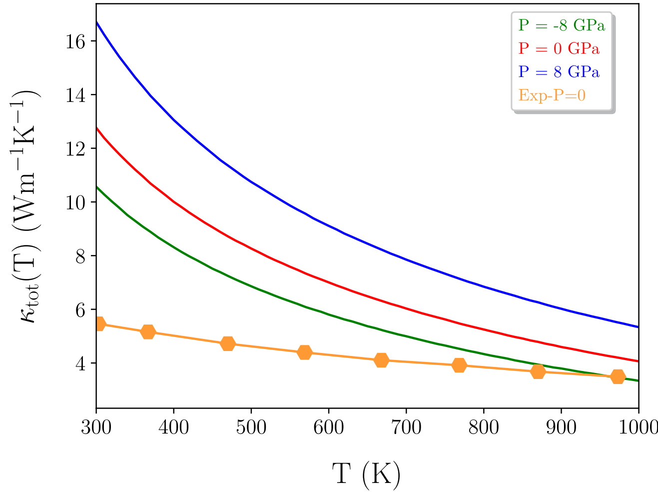

FIG. 11. Calculated total thermal conductivity (κ_{tot}) of TaFeSb at various pressures, for $n = 20 \times 10^{20}$ cm^{-3}. Experimental results [6] for $Ta_{0.84}Ti_{0.16}FeSb$ at zero pressure are also shown.

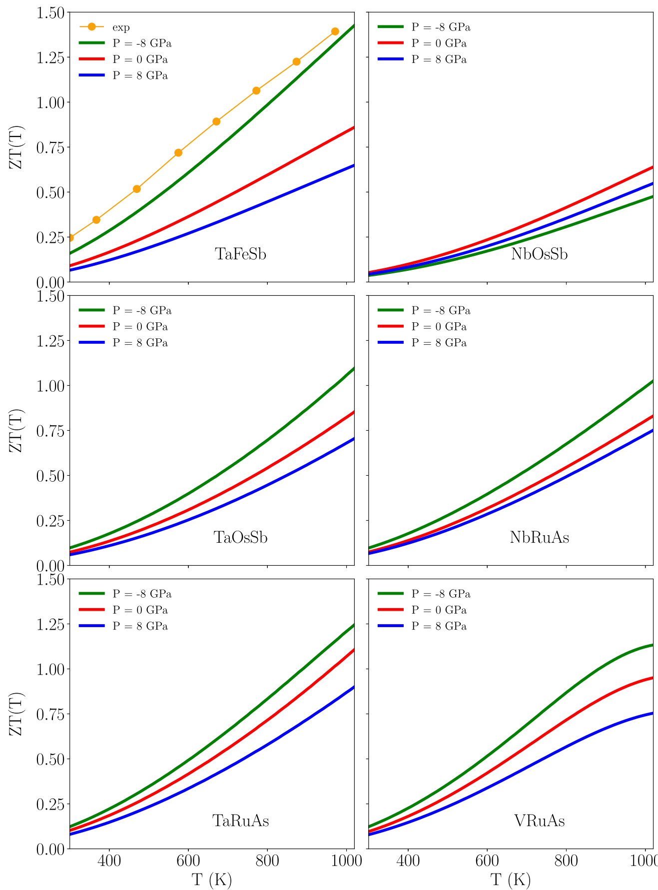

FIG. 12. Calculated figure of merit ZT of TaFeSb, TaOsSb, TaRuAs, NbOsSb, NbRuAs, and VRuAs as a function of temperature, for various pressures and with $n = 20 \times 10^{20}$ cm^{-3}. Experimental results [6] for $Ta_{0.84}Ti_{0.16}FeSb$ at zero pressure are also shown.

the reference curve, but the high-temperature discrepancies are more pronounced and start at about 600 K. Overall, these curves demonstrate that the effects of an overestimated coherence in the undoped system, due to neglecting explicit scattering centers, cancel out in the final calculation of the figure of merit. Considering that small discrepancies may also arise from slightly different computational details between the standard unit cell and the supercells, we can conclude that our modeling of the volumetric changes is capable of describing the thermoelectric properties of $TaRuAs_{0.875}Bi_{0.125}$ rather well.

VI. CONCLUSION

By utilizing a combination of density functional and Boltzmann theories, we investigated the effect of negative and positive pressure on the electronic and thermoelectric properties of the HH compounds TaFeSb, MOsSb (M = Ta, Nb), and NRuAs (N = Ta, Nb, V). All these materials are found to be indirect band-gap semiconductors in their ground state. With the exception of TaRuAs, volume change does not affect the location of the VBM and CBM. Conversely, the size of the band gap decreases upon volume compression in TaOsSb, NbOsSb, NbRuAs, and VRuAs, while the opposite trend is observed in TaFeSb and TaRuAs. A similar behavior is observed for the Seebeck coefficient. Among the compounds, TaFeSb stands out for having the largest band gap, and consequently the largest Seebeck coefficient, independently of the applied pressure. The analysis of electrical conductivity, power factor, and lattice thermal conductivity reveals that they are all increased by volume compression, reflecting the larger bandwidth observed for valence and conduction bands. All these properties are then entering into the figure of merit, which settles the final thermoelectric efficiency. Volume extension (compression) is found to increase (decrease) the thermoelectric efficiency of TaFeSb, TaOsSb, NbRuAs, and VRuAs compounds. Due to the more complex behavior outlined above, the thermoelectric efficiency of TaRuAs increases upon volume increase at low and intermediate temperatures, but acquires an irregular behavior at higher temperatures, which we trace back to the thermal conductivity. In contrast to the other compounds, the best thermoelectric efficiency of NbOsSb is observed at zero pressure, as neither compression or extension can improve the properties of the ground state. Overall, our calculations demonstrate that TaRuAs is the best compound among those investigated, due to having the highest power factor and the lowest (lattice) thermal conductivity. Our results predict TaRuAs to be a good candidate for more detailed experimental investigation toward the implementation for thermoelectric applications with high efficiency.

Although our study intends to evaluate the response of several HH compounds to volumetric changes, the most practical way to enforce the latter is doping with selected chemical elements. To verify the predictive ability of our approach in modeling volumetric changes induced by doping, as well as to provide a more realistic test-case as a suggestion to the experimentalists, we also investigated the thermoelectric properties of $TaRuAs_{0.875}Bi_{0.125}$. The favorable comparison between these results and those obtained for undoped TaRuAs under a chemical pressure of −2 or −4 GPa suggests that

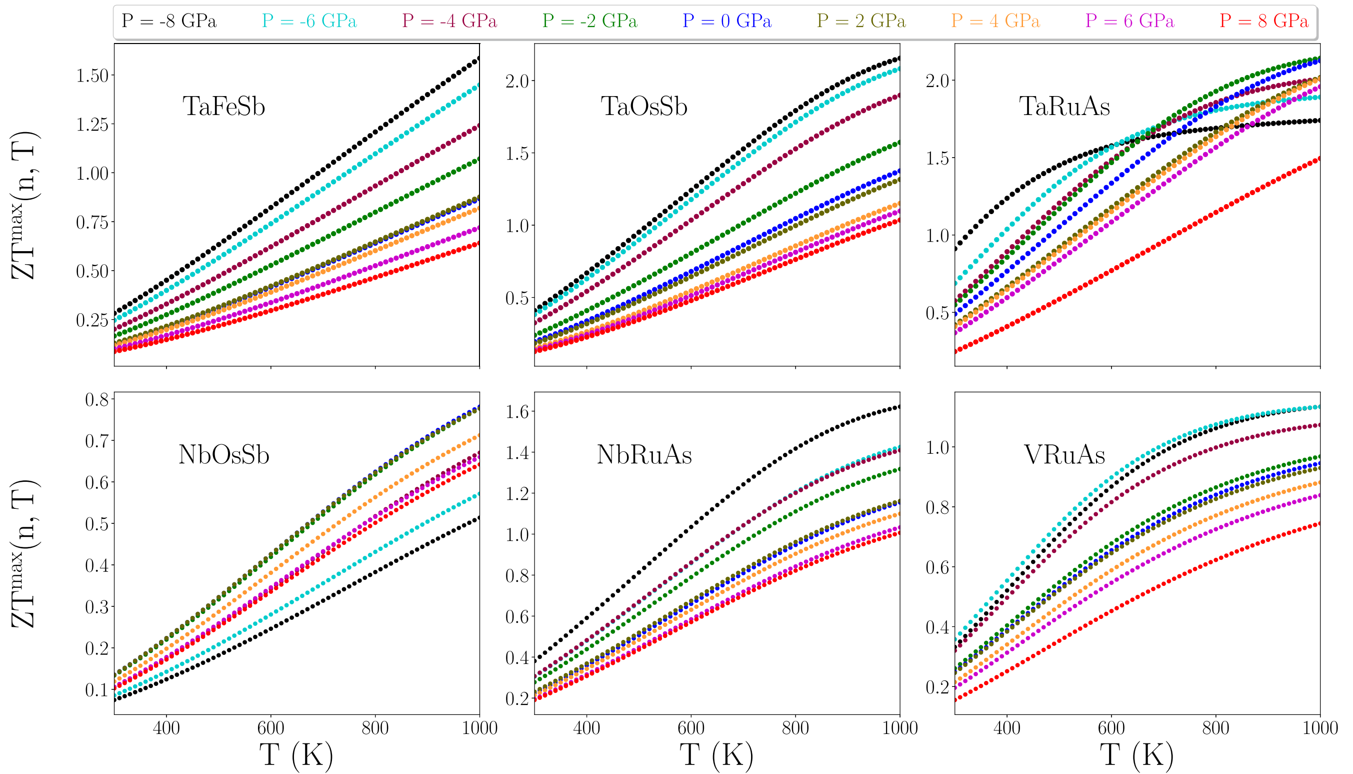

FIG. 13. Maximum value of the figure of merit per temperature ($Z^{\max}T$) of TaFeSb, TaOsSb, TaRuAs, NbOsSb, NbRuAs, and VRuAs with respect to a varying carrier concentration, as a function of temperature and for pressures from −8 to 8 GPa.

volumetric changes alone may be sufficient to be used as a guideline for material optimization in thermoelectricity. The discrepancies associated with ignoring the quantum effects beyond the chemical pressure are found to be moderate and, most importantly, cancel each other in the final determination of the figure of merit. Considering that full *ab initio* calculations for realistic alloys are not feasible for data mining or large-scale optimization, because of their prohibitive computational cost, our suggestion to consider the chemical pressure on undoped materials is a clear improvement with respect to ignoring these effects altogether.

Finally, it is important to stress that volumetric changes may not only be induced via doping or direct hydrostatic pressure, but also via a variation of temperature. HH compounds

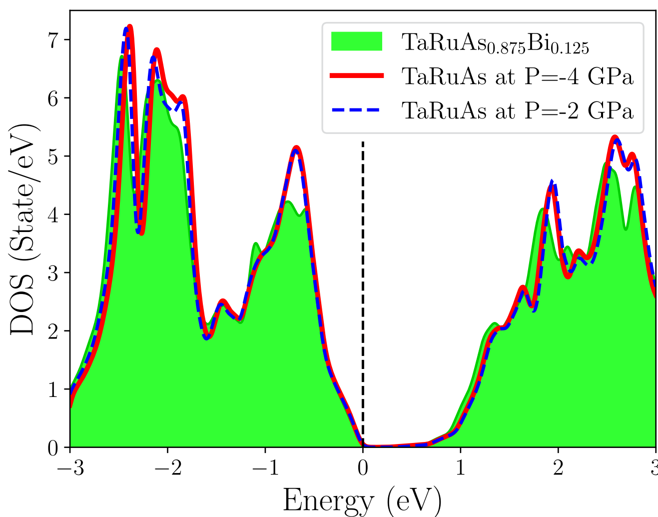

FIG. 14. Total density of states of $TaRuAs_{0.875}Bi_{0.125}$ at zero pressure and undoped TaRuAs at −2 and −4 GPa. The curves are normalized per formula unit, and the Fermi level is at zero energy.

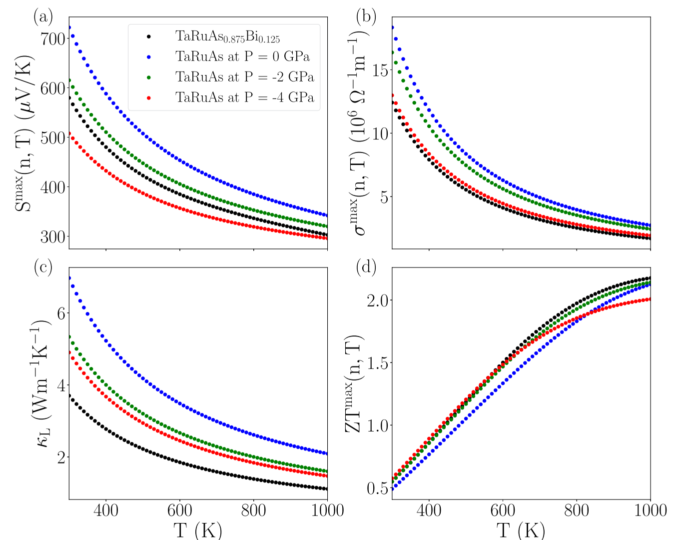

FIG. 15. Maximum values of (a) Seebeck coefficient $S^{\max}$, (b) electrical conductivity $\sigma^{\max}$, and (d) figure of merit $Z^{\max}T$, for $TaRuAs_{0.875}Bi_{0.125}$ at zero pressure and TaRuAs at various pressures, as a function of temperature. Panel (c) shows the corresponding lattice thermal conductivity κ_L.

for thermoelectricity have been reported to have an average linear thermal expansion coefficient as high as 13×10^{-6} K^{-1} [86–88]. In terms of unit-cell volumes, this means that ZrNiSn, TiNiSn, and HfNiSn undergo an increase between 2% and 2.5% when going from 313 to 963 K [86]. Therefore, our results suggest that the present state-of-the-art computational theory of thermoelectricity, whose starting point is the crystal structure at zero temperature, may deviate from the experimental reality quite substantially for temperatures above room temperature. Another aspect associated with induced changes of volume is the connection to the piezoelectric effect, which may be sizable in HH compounds [89,90]. In the context of our study, one may wonder if it is possible to combine piezoelectric and thermoelectric effects. As a matter of fact, several studies suggested this possibility during the past decade in order to increase the efficiency of devices for energy harvesting, hence increasing their applications in real life [90–95]. Developing a theory that allows us to take into account the concomitant action of all direct and indirect effects in hybrid devices is going to be a significant challenge for the material science community.

As a future outlook, we note that the approach presented here is not limited to HH compounds, but can be applied to any generic thermoelectric material where a substantial volumetric change is expected from achievable doping. Among recently discovered systems, the HH compound ZrNiBi seems very interesting to investigate, due to the peculiar characteristics of its electronic structure, especially in the presence of vacancies [96]. Mg_3Bi_2-based materials can be doped with atoms of very different size [97] and are therefore ideal targets for our volumetric analysis. Instead, $AgSbTe_2$ is a compound where doping induces marked changes in the thermoelectric properties, which are mainly driven by disorder [98]. Our approach may be useful to clarify the role played by purely volumetric effects and quantum effects separately. Finally, Ni_xAu_{1-x} alloys provide an (almost) unique example of a metallic system with a large thermoelectric effect, enabled by strong intrinsic interband scattering [99]. Understanding the variation of these mechanisms with respect to volume change may help in optimizing the thermoelectric properties in metallic systems as well.

ACKNOWLEDGMENTS

M.Y.K., S.M.V.A., and I.D.M. are grateful for the financial support from the Iran National Science Foundation (INSF) under Grant No. 99002221. I.D.M. acknowledges financial support from the European Research Council (ERC), Synergy Grant FASTCORR, Project No. 854843. The work of I.D.M. is also supported by the appointment to the JRG program at the APCTP through the Science and Technology Promotion Fund and Lottery Fund of the Korean Government, as well as by the Korean Local Governments, Gyeongsangbuk-do Province, and Pohang City. The computational work was enabled by resources provided by the Swedish National Infrastructure for Computing (SNIC) at the Uppsala Multidisciplinary Center for Advanced Computational Science (UPPMAX) and the Center for High Performance Computing (PDC) in Stockholm, Sweden, partially funded by the Swedish Research Council through Grant Agreement No. 2018-05973. Additional calculations were also performed on the local computing clusters (TC and Prime) at the Institute of Physics, Nicolaus Copernicus University, and we are grateful to Szymon Śmiga for access and support.

[1] E. A. Maciá Barber, *Thermoelectric Materials: Advances and Applications* (Pan Stanford, Singapore, 2015).
[2] B. Jiang, Y. Yu, J. Cui, X. Liu, L. Xie, J. Liao, Q. Zhang, Y. Huang, S. Ning, B. Jia, B. Zhu, S. Bai, L. Chen, S. J. Pennycook, and J. He, Science **371**, 830 (2021).
[3] C. J. Perez, M. Wood, F. Ricci, G. Yu, T. Vo, S. K. Bux, G. Hautier, G.-M. Rignanese, G. J. Snyder, and S. M. Kauzlarich, Sci. Adv. **7**, eabe9439 (2021).
[4] W. Ren, Y. Sun, D. Zhao, A. Aili, S. Zhang, C. Shi, J. Zhang, H. Geng, J. Zhang, L. Zhang, J. Xiao, and R. Yang, Sci. Adv. **7**, eabe0586 (2021).
[5] J. Zhang, L. Song, and B. B. Iversen, npj Comput Mater **5**, 76 (2019).
[6] H. Zhu, J. Mao, Y. Li, J. Sun, Y. Wang, Q. Zhu, G. Li, Q. Song, J. Zhou, Y. Fu, R. He, T. Tong, Z. Liu, W. Ren, L. You, Z. Wang, J. Luo, A. Sotnikov, J. Bao, K. Nielsch, G. Chen, D. J. Singh, and Z. Ren, Nat. Commun. **10**, 270 (2019).
[7] B. Jiang, W. Wang, S. Liu, Y. Wang, C. Wang, Y. Chen, L. Xie, M. Huang, and J. He, Science **377**, 208 (2022).
[8] Y. Jiang, J. Dong, H.-L. Zhuang, J. Yu, B. Su, H. Li, J. Pei, F.-H. Sun, M. Zhou, H. Hu, J.-W. Li, Z. Han, B.-P. Zhang, T. Mori, and J.-F. Li, Nat. Commun. **13**, 6087 (2022).
[9] Y. Gan, G. Wang, J. Zhou, and Z. Sun, npj Comput. Mater. **7**, 176 (2021).
[10] G. A. Naydenov, P. J. Hasnip, V. K. Lazarov, and M. I. J. Probert, J. Phys.: Mater. **2**, 035002 (2019).
[11] J.-H. Yang, Q. Yuan, H. Deng, S.-H. Wei, and B. I. Yakobson, J. Phys. Chem. C **121**, 123 (2017).
[12] S. Sarkar, O. Eriksson, D. D. Sarma, and I. Di Marco, Phys. Rev. B **105**, 184201 (2022).
[13] T. Dan, A. Mohanty, A. Dutta, R. M. Varma, S. Sarkar, I. Di Marco, O. Eriksson, E. Welter, S. Pollastri, L. Olivi, K. R. Priolkar, and D. D. Sarma, Phys. Rev. B **104**, 184113 (2021).
[14] A. Grytsiv, V. Romaka, N. Watson, G. Rogl, H. Michor, B. Hinterleitner, S. Puchegger, E. Bauer, and P. Rogl, Intermetallics **111**, 106468 (2019).
[15] J. Zhu, F. Liu, G. B. Stringfellow, and S.-H. Wei, Phys. Rev. Lett. **105**, 195503 (2010).
[16] D. Weber, J. Lin, A. Pokle, K. Volz, J. Janek, T. Brezesinski, and M. Bianchini, J. Electrochem. Soc. **169**, 030540 (2022).
[17] M. S. Park, J.-H. Song, J. E. Medvedeva, M. Kim, I. G. Kim, and A. J. Freeman, Phys. Rev. B **81**, 155211 (2010).
[18] J. L. Baker, C. Park, C. Kenney-Benson, V. K. Sharma, V. Kanchana, G. Vaitheeswaran, C. J. Pickard, A. Cornelius, N. Velisavljevic, and R. S. Kumar, J. Phys. Chem. Lett. **12**, 1046 (2021).
[19] S. Ning, S. Huang, Z. Zhang, R. Zhang, N. Qi, and Z. Chen, Phys. Chem. Chem. Phys. **22**, 14621 (2020).

[20] P. Govindaraj, M. Sivasamy, K. Murugan, K. Venugopal, and P. Veluswamy, RSC Adv. **12**, 12573 (2022).
[21] S. Mukherjee, A. Nag, V. Kocevski, P. K. Santra, M. Balasubramanian, S. Chattopadhyay, T. Shibata, F. Schaefers, J. Rusz, C. Gerard, O. Eriksson, C. U. Segre, and D. D. Sarma, Phys. Rev. B **89**, 224105 (2014).
[22] P. Qiu, X. Huang, X. Chen, and L. Chen, J. Appl. Phys. **106**, 103703 (2009).
[23] M. Yazdani-Kachoei, S. Rahimi, R. Ebrahimi-Jaberi, J. Nematollahi, and S. Jalali-Asadabadi, Sci. Rep. **12**, 663 (2022).
[24] M. Yazdani-Kachoei and S. Jalali-Asadabadi, RSC Adv. **9**, 36182 (2019).
[25] Y. Takaesu, N. Aso, Y. Tamaki, M. Hedo, T. Nakama, K. Uchima, Y. Ishikawa, K. Deguchi, and N. K. Sato, J. Phys.: Conf. Ser. **273**, 012058 (2011).
[26] N. V. Morozova, I. V. Korobeinikov, and S. V. Ovsyannikov, J. Appl. Phys. **125**, 220901 (2019).
[27] Q. Ren, C. Fu, Q. Qiu, S. Dai, Z. Liu, T. Masuda, S. Asai, M. Hagihala, S. Lee, S. Torri, T. Kamiyama, L. He, X. Tong, C. Felser, D. J. Singh, T. Zhu, J. Yang, and J. Ma, Nat. Commun. **11**, 3142 (2020).
[28] X. Ye, Z. Feng, Y. Zhang, G. Zhao, and D. J. Singh, Phys. Rev. B **105**, 104309 (2022).
[29] K. Ciesielski, K. Synoradzki, I. Veremchuk, P. Skokowski, D. Szymański, Y. Grin, and D. Kaczorowski, Phys. Rev. Appl. **14**, 054046 (2020).
[30] M. Zeeshan, T. Nautiyal, J. van den Brink, and H. C. Kandpal, Phys. Rev. Mater. **2**, 065407 (2018).
[31] M. Yazdani-Kachoei and S. Jalali-Asadabadi, J. Alloys Compd **828**, 154287 (2020).
[32] T. Graf, C. Felser, and S. S. P. Parkin, Prog. Solid State Chem. **39**, 1 (2011).
[33] R. A. de Groot, F. M. Mueller, P. G. van Engen, and K. H. J. Buschow, Phys. Rev. Lett. **50**, 2024 (1983).
[34] F. G. Aliev, N. B. Brandt, V. V. Moshchalkov, V. V. Kozyrkov, R. V. Skolozdra, and A. I. Belogorokhov, Z. Phys. B **75**, 167 (1989).
[35] F. Aliev, V. Kozyrkov, V. Moshchalkov, R. Scolozdra, and K. Durczewski, Z. Phys. B **80**, 353 (1990).
[36] F. G. Aliev, Phys. B: Condens. Matter **171**, 199 (1991).
[37] S. Öğüt and K. M. Rabe, Phys. Rev. B **51**, 10443 (1995).
[38] F. Casper, T. Graf, S. Chadov, B. Balke, and C. Felser, Semicond. Sci. Technol. **27**, 063001 (2012).
[39] K. Manna, Y. Sun, L. Muechler, J. Kübler, and C. Felser, Nat. Rev. Mater. **3**, 244 (2018).
[40] R. Liu, Y. Xing, J. Liao, X. Xia, C. Wang, C. Zhu, F. Xu, Z.-G. Chen, L. Chen, J. Huang, and S. Bai, Nat. Commun. **13**, 7738 (2022).
[41] R. Tranås, O. M. Løvvik, O. Tomic, and K. Berland, Comput. Mater. Sci **202**, 110938 (2022).
[42] J. Akinlami, O. Odeyemi, M. Omeike, and G. Adebayo, Mater. Sci. Semicond. Proc. **148**, 106837 (2022).
[43] W. Kohn and L. J. Sham, Phys. Rev. **140**, A1133 (1965).
[44] P. Hohenberg and W. Kohn, Phys. Rev. **136**, B864 (1964).
[45] J. Chelikowsky and S. Louie, *Quantum Theory of Real Materials*, The Springer International Series in Engineering and Computer Science (Springer, US, 1996).
[46] See Supplemental Material at http://link.aps.org/supplemental/10.1103/PhysRevMaterials.7.104602. for additional details on the calculations, as well as the results of the optimized lattice parameters and elastic properties.
[47] M. Shafiq, S. Arif, I. Ahmad, S. J. Asadabadi, M. Maqbool, and H. Rahnamaye Aliabad, J. Alloys Compd **618**, 292 (2015).
[48] F. Shi, M. S. Si, J. Xie, K. Mi, C. Xiao, and Q. Luo, J. Appl. Phys. **122**, 215701 (2017).
[49] F. Mouhat and F.-X. Coudert, Phys. Rev. B **90**, 224104 (2014).
[50] J. Ma, V. I. Hegde, K. Munira, Y. Xie, S. Keshavarz, D. T. Mildebrath, C. Wolverton, A. W. Ghosh, and W. H. Butler, Phys. Rev. B **95**, 024411 (2017).
[51] G. K. H. Madsen, P. Blaha, K. Schwarz, E. Sjöstedt, and L. Nordström, Phys. Rev. B **64**, 195134 (2001).
[52] P. Blaha, K. Schwarz, G. K. H. Madsen, D. Kvasnicka, and J. Luitz, WIEN2k: *An Augmented Plane Waves plus Local Orbitals Program for Calculating Crystal Properties* (Vienna University of Technology, Austria, 2001).
[53] S.-D. Guo, J. Alloys Compd. **663**, 128 (2016).
[54] J. Umukoro, O. Omagbemi, and O. Osafile, J. Phys. Chem. Res. **4**, 148 (2022).
[55] H. J. Monkhorst and J. D. Pack, Phys. Rev. B **13**, 5188 (1976).
[56] J. P. Perdew, K. Burke, and M. Ernzerhof, Phys. Rev. Lett. **77**, 3865 (1996).
[57] O. Rubel, F. Tran, X. Rocquefelte, and P. Blaha, Comput. Phys. Commun **261**, 107648 (2021).
[58] M. Jamal, M. Bilal, I. Ahmad, and S. Jalali-Asadabadi, J. Alloys Compd **735**, 569 (2018).
[59] G. K. H. Madsen, J. Carrete, and M. J. Verstraete, Comput. Phys. Commun. **231**, 140 (2018).
[60] Z. Shuai, L. Wang, and C. Song, *Theory of Charge Transport in Carbon Electronic Materials*, SpringerBriefs in Molecular Science (Springer, Berlin, 2012).
[61] J. Ziman, *Electrons and Phonons: The Theory of Transport Phenomena in Solids*, International Series of Monographs on Physics (Oxford University Press, Oxford, 2001).
[62] W. Li, J. Carrete, N. A. Katcho, and N. Mingo, Comput. Phys. Commun **185**, 1747 (2014).
[63] T. Jia, G. Chen, and Y. Zhang, Phys. Rev. B **95**, 155206 (2017).
[64] D. T. Morelli, V. Jovovic, and J. P. Heremans, Phys. Rev. Lett. **101**, 035901 (2008).
[65] G. Kresse and J. Hafner, Phys. Rev. B **47**, 558 (1993).
[66] G. Kresse and J. Furthmüller, Comput. Mater. Sci **6**, 15 (1996).
[67] A. Togo, L. Chaput, and I. Tanaka, Phys. Rev. B **91**, 094306 (2015).
[68] A. Togo, J. Phys. Soc. Jpn. **92**, 012001 (2023).
[69] F. D. Murnaghan, Proc. Natl. Acad. Sci. USA **30**, 244 (1944).
[70] P. Qiu, J. Yang, X. Huang, X. Chen, and L. Chen, Appl. Phys. Lett. **96**, 152105 (2010).
[71] S. R. Culp, S. J. Poon, N. Hickman, T. M. Tritt, and J. Blumm, Appl. Phys. Lett. **88**, 042106 (2006).
[72] S. Bhattacharya and G. K. H. Madsen, J. Mater. Chem. C **4**, 11261 (2016).
[73] F. Tran and P. Blaha, Phys. Rev. Lett. **102**, 226401 (2009).
[74] D. Koller, F. Tran, and P. Blaha, Phys. Rev. B **83**, 195134 (2011).
[75] P. Dey and B. Dutta, Phys. Rev. Mater. **5**, 035407 (2021).
[76] A. Saini, R. Singh, and R. Kumar, Pressure induced enhancement in the power factor of p-type LiScSi half-Heusler alloy,

edited by V. K. Sharma, C. L. Prajapat, and S.M. Yusuf (AIP, New York, 2020), p. 030454.

[77] S. Huang, X. Liu, W. Zheng, J. Guo, R. Xiong, Z. Wang, and J. Shi, J. Mater. Chem. A **6**, 20069 (2018).

[78] H. J. Goldsmid and J. W. Sharp, J. Electron. Mater. **28**, 869 (1999).

[79] D. M. Hoat, Comput. Mater. Sci. **159**, 470 (2019).

[80] T. Sekimoto, K. Kurosaki, H. Muta, and S. Yamanaka, J. Alloys Compd. **407**, 326 (2006).

[81] H.-H. Xie, J.-L. Mi, L.-P. Hu, N. Lock, M. Chirstensen, C.-G. Fu, B. B. Iversen, X.-B. Zhao, and T.-J. Zhu, CrystEngComm **14**, 4467 (2012).

[82] G. H. Fecher, E. Rausch, B. Balke, A. Weidenkaff, and C. Felser, Phys. Status Solidi A **213**, 716 (2016).

[83] D. V. Livanov and A. V. Sergeev, Phys. Rev. B **48**, 13137 (1993).

[84] M. Fava, B. Dongre, J. Carrete, A. van Roekeghem, G. K. H. Madsen, and N. Mingo, Phys. Rev. B **103**, 174112 (2021).

[85] W. Ren, X. Shi, Z. Wang, and Z. Ren, Mater. Today Phys **25**, 100704 (2022).

[86] D.-y. Jung, K. Kurosaki, C.-e. Kim, H. Muta, and S. Yamanaka, J. Alloys Compd. **489**, 328 (2010).

[87] T. Sekimoto, K. Kurosaki, H. Muta, and S. Yamanaka, Mater. Trans. **48**, 2079 (2007).

[88] D. A. Ferluccio, B. F. Kennedy, S. A. Barczak, S. R. Popuri, C. Murray, M. Pollet, and J.-W. G. Bos, J. Phys.: Energy **3**, 035001 (2021).

[89] A. Roy, J. W. Bennett, K. M. Rabe, and D. Vanderbilt, Phys. Rev. Lett. **109**, 037602 (2012).

[90] Z. A. A. R. Almaghbash, O. Arbouche, A. Dahani, A. Cherifi, M. Belabbas, A. Zenati, H. Mebarki, and A. Hussain, Int. J. Thermophys. **42**, 5 (2021).

[91] S. Chen, X. Chen, Z. Zeng, H. Geng, and H. Yin, Phys. Chem. Chem. Phys. **23**, 26955 (2021).

[92] F. Yang, J. Wu, A. Suwardi, Y. Zhao, B. Liang, J. Jiang, J. Xu, D. Chi, K. Hippalgaonkar, J. Lu, and Z. Ni, Adv. Mater **33**, 2004786 (2021).

[93] V. Andrei, K. Bethke, and K. Rademann, Energy Environ. Sci. **9**, 1528 (2016).

[94] D. S. Montgomery, C. A. Hewitt, and D. L. Carroll, Appl. Phys. Lett. **108**, 263901 (2016).

[95] G. Wang, H. Yin, S.-D. Guo, and Y. S. Ang, Front. Phys. **11**, 1244195 (2023).

[96] W. Ren, W. Xue, G. Guo, R. He, L. Deng, S. Song, A. Sotnikov, K. Nielsch, J. van den Brink, G. Gao, A. Chen, Y. Han, J. Wu, C.-W. Chu, Z. Wang, Y. Wang, and Z. Ren, Nat. Commun. **14**, 4722 (2023).

[97] J. Mao, H. Zhu, Z. Ding, Z. Liu, G. A. Gamage, G. Chen, and Z. Ren, Science **365**, 495 (2019).

[98] S. Roychowdhury, T. Ghosh, R. Arora, M. Samanta, L. Xie, N. K. Singh, A. Soni, J. He, U. V. Waghmare, and K. Biswas, Science **371**, 722 (2021).

[99] F. Garmroudi, M. Parzer, A. Riss, C. Bourgès, S. Khmelevskyi, T. Mori, E. Bauer, and A. Pustogow, Sci. Adv. **9**, eadj1611 (2023).